Electronic and magnetic properties of $(Zn_{1-x}V_x)O$ diluted magnetic semiconductors elucidated from x-ray magnetic circular dichroism at V $L_{2,3}$ edges and first-principles calculations

L. V. Bekenov,[1,2] V. N. Antonov,[2,3,*] S. Ostanin,[1] A. N. Yaresko,[3] I. V. Maznichenko,[4,5] W. Hergert,[4] I. Mertig,[1,4] and A. Ernst[1,†]

[1]*Max-Planck Institut für Mikrostrukturphysik, Weinberg 2, D-06120 Halle, Germany*
[2]*Institute of Metal Physics, 36 Vernadsky Street, 03142 Kiev, Ukraine*
[3]*Max-Planck-Institut für Festkörperforschung, Heisenberg Strasse 1, D-70569 Stuttgart, Germany*
[4]*Institut für Physik, Martin-Luther-Universität Halle-Wittenberg, D-06099 Halle, Germany*
[5]*Institute of Physics at Southern Federal University, 194 Stachky Avenue, Rostov-on-Don 344090, Russia*

(Received 10 June 2011; revised manuscript received 27 September 2011; published 17 October 2011)

The electronic structure of (Zn,V)O dilute magnetic semiconductors (DMSs) was investigated theoretically from first principles, using the fully relativistic Dirac linear muffin-tin orbital band structure method and the Korringa-Kohn-Rostoker Green's function approach within the local spin-density approximation. X-ray magnetic circular dichroism (XMCD) spectra at the V $L_{2,3}$ edges were calculated. Comparing the experimental results and the theoretical simulations we discuss possible crystal and magnetic structures of (Zn,V)O and reach the best agreement with the experimental XMCD spectra for the antiferromagnetically ordered DMSs in the presence of an oxygen vacancy. The corresponding structure was used to determine the electronic and magnetic properties of (Zn,V)O.

DOI: 10.1103/PhysRevB.84.134421 PACS number(s): 75.50.Cc, 71.20.Lp, 71.15.Rf

I. INTRODUCTION

Zinc oxide (ZnO), a representative II-VI compound semiconductor, has attracted considerable attention because of its numerous attractive properties, such as the direct wide band gap (3.37 eV), large exciton binding energy (60 meV at room temperature), good piezoelectric characteristics, chemical stability, and biocompatibility. This offers a variety of applications, e.g., energy efficiency windows, smart windows, and electrodes for solar cells, as well as flat-panel displays, etc. (Ref. 1). Recently, ZnO became an interesting candidate as a dilute magnetic semiconductor (DMS) with potentially high Curie temperature (T_C),[2] aiming at practical applications in spintronics devices. After the first report of $T_C \sim 280$ K in $(Zn_{1-x}Co_x)O$,[3] there have been many subsequent publications on ZnO-based DMSs, which also show relatively high T_C (for a review, see Ref. 4).

Recently, it has been reported that V doping can cause ferromagnetism (FM) in ZnO. However, not much work has been done on the system and the results obtained so far are rather controversial. For instance, Saeki and co-workers[5,6] observed ferromagnetic behavior at $T_C > 350$ K while Hong *et al.*[7,8] found room-temperature ferromagnetism along with spin-glass behavior seen at low temperatures. Meanwhile, Venkatesan *et al.*[9] and Neal *et al.*[10] have reported the observation of anisotropic ferromagnetism and room-temperature ferromagnetism in V-doped ZnO thin films, respectively. The latter authors[10] also reported paramagnetism at 10 K when the sample was subjected to rapid thermal annealing which agrees with the results of Saeki *et al.* (Ref. 11). On the other hand, Ramachandran *et al.*[12] have reported that (Zn,V)O is not ferromagnetic above 10 K. The most recent studies indicate the coexistence of the Curie-Weiss paramagnetic (PM) and the antiferromagnetic (AFM) state for the V ions in ZnO thin films.[13] Besides, ferromagnetism was not observed down to 5 K in V-doped ZnO single crystals.[14] These contradictory experimental results suggest that the magnetic coupling in the (Zn,V)O system may be extremely sensitive to the sample preparation conditions.

All theoretical results[15–20] reported until recently are almost equally conflicting. For example, Sato and Katayama-Yoshida,[17] using the Korringa-Kohn-Rostoker (KKR) coherent potential approximation within the local density approximation (LDA) to the exchange-correlation energy, obtained ferromagnetism in V-doped ZnO, while Kang *et al.*[19] suggested the antiferromagnetic solution for the system using the full-potential linear muffin-tin orbital method within the generalized gradient approximation (GGA). Wang *et al.*[20] have presented recently systematic *ab initio* calculations of the electronic and magnetic properties of V-doped ZnO in both bulk and thin films. The structural relaxation and total energy calculations have been carried out using the spin polarized option of density functional theory (DFT). Vanadium substitutions at the Zn host sites show minor selectivity of the site occupancy. More importantly, after relaxation of both the (Zn,V)O bulk and subsurface layers of the thin film, the ferromagnetic, ferrimagnetic, and antiferromagnetic configurations are energetically nearly equivalent. On the other hand, V atoms couple ferromagnetically when they occupy the surface sites of the thin film.

As we mentioned above the physical properties of ZnO might be very sensitive to different kinds of defects in the crystal. In spite of numerous experimental studies, there is still controversy concerning the relevant native defects of this oxide. Single-crystal ZnO has always been observed to contain metal excess (or oxygen deficiency).[21] The metal excess can be accommodated in part by the presence of zinc interstitials or oxygen vacancies. Experiments have been inconclusive with respect to the predominant defect. Results presented in the literature assume both one or the other situation and different interpretations have even been taken on the same set of experimental data (see, for example, Ref. 22). Interstitial

zinc atoms have been proposed as the dominant defect on the basis of ionic diffusion or size considerations.[21,23–25] Other authors, based on calculation of reaction rates,[22] diffusion experiments,[26] or electrical conductivity and Hall effect measurements,[27] concluded that oxygen vacancies were the predominant defects.

A series of calculations, performed in the framework of density functional theory, have been devoted to native defects in ZnO.[28–31] The formation energies and defect levels are discussed especially in connection to the doping problem and defect-driven magnetism. Kohan *et al.*[30] have studied the relevant defects that may be present in ZnO. By using the plane-wave soft-pseudopotential technique together with the supercell approach they have found that the dominant native defects in ZnO are oxygen and zinc vacancies. Yuming *et al.*[15] performed theoretical studies using the full-potential linear muffin-tin orbital (FPLMTO) method on the native shallow donor in ZnO. They have reported that the vacancy of O produces occupied defect states ∼1.3 eV below the bottom conduction band, while the vacancy of Zn and interstitial Zn produces shallow acceptor states of ∼0.3 eV above the top of the valence band and shallow donor states of ∼0.5 eV below the bottom of the conduction band, respectively. In order to investigate the electronic properties of the impurity and those of O or Zn vacancy sites in wurtzite ZnO, Kang *et al.*[19] have calculated the electronic structures for the DMS $(Zn_{1-x}M_x)O$ (M = V or Mn) using the FPLMTO method. They have discussed the effect of the interaction between the magnetic impurity V and the defects of O or Zn in ZnO on the band gap.

One of the main problems of theoretical considerations of DMSs is the lack of information concerning the crystal structure and the chemical composition. Usually DMSs are fabricated using epitaxial-growth techniques under far from equilibrium conditions. Therefore, an exact determination of their crystal structure is often not possible either with experiments or first-principles methods. One way to get more insight into the particular properties of DMS is an *ab initio* simulation and a direct comparison of it with experiment. First-principles methods can often provide an adequate description of many observable properties. The crystal structure can be parametrized in such simulations. By varying atomic positions and the chemical composition, one can achieve an acceptable fit of a particular quantity. The structural information, obtained this way, can be used for investigations of other properties of the considered system. One of the observable quantities, which can be adequately calculated for many systems from first principles, is the x-ray absorption spectrum (XAS) as well as x-ray magnetic circular dichroism (XMCD), which is the difference of the x-ray absorption spectra with opposite (left and right) directions of circular polarization.

In the present study, we focus attention on x-ray absorption spectra and x-ray magnetic circular dichroism of (Zn,V)O DMSs. The XAS at the V K edge was measured by several groups.[13,32] Field and temperature dependencies of the XAS and XMCD spectra at the V $L_{2,3}$ edges in the $(Zn_{1-x}V_x)O$ ($x = 0.05$) were reported by Ishida *et al.*[13] They found a linear increase of the XMCD signal with external magnetic field H which indicates that the paramagnetic signal dominates the XMCD signal and that the ferromagnetic component is small, consistent with their magnetization measurements. The majority of the V ions were presumably strongly coupled antiferromagnetically. They estimate that ∼10% of the V ions were paramagnetic, ∼90% were presumably strongly antiferromagnetically coupled, and the ferromagnetic component was below the detection limit of XMCD. In our study we simulate the XAS and XMCD spectra from first principles by varying the crystal structure, the chemical composition, and the magnetic order systematically, searching for optimal agreement. The obtained information is used for the extensive study of the electronic and magnetic properties of (Zn,V)O DMS.

The paper is organized as follows. Section II presents structural models for (Zn,V)O DMSs used in the present work and the details of the calculations. Section III is devoted to our simulations of XMCD experiments and to the electronic structure as well as the magnetic properties of the DMSs calculated with the fully relativistic LMTO band structure method and the KKR Green's function approach. The results are compared with available experimental data. Finally, the results are summarized in Sec. IV.

II. STRUCTURAL MODEL AND COMPUTATIONAL DETAILS

The constituents in the (Zn,V)O compound have the following nominal atomic structures: $[Ar]3d^{10}4s^2$ for Zn, $[Ar]3d^3 4s^2$ for V, and $[He]2s^2 2p^4$ for O. The most stable and therefore most common position of V in the ZnO host lattice is at the Zn site where its two $4s$ electrons can participate in crystal bonding in the same way as the two Zn $4s$ electrons. The theoretical calculations[20] and experimental measurements[5–9] suggest that there is no clear site preference for the V atoms in bulk ZnO and V doping in ZnO is almost homogeneous.

The calculations of the electronic structure of the (Zn,V)O DMSs were performed for $3a \times 3a \times 1c$, $3a \times 3a \times 2c$, and $4a \times 4a \times 1c$, supercells of the wurtzite-type ZnO unit cell with one or two of the Zn ions replaced by V. The supercell calculations were performed for the compositions $x = 0.0556$ (1/18), $x = 0.03125$ (1/32), and $x = 0.02778$ (1/36) using the simple trigonal $P3m1$ (No. 156) space group. The substitutional $(Zn_{1-x}V_x)O$ positions are illustrated in Fig. 1 for a 36-atom ZnO unit cell containing two substitutional V atoms ($x = 0.1111$) for the largest possible V-V interatomic distance of 5.53 Å. The V atom has four O nearest neighbors:

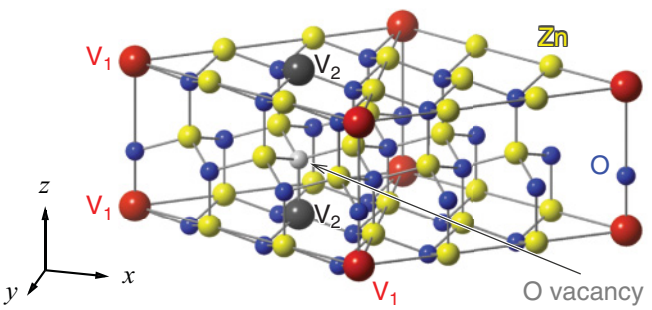

FIG. 1. (Color online) Schematic representation of the (Zn,V)O structure with two substituted V atoms with the largest possible V-V interatomic distance for a giving concentration (see text).

three O atoms at the distance of 1.949 Å and one O atom at 1.950 Å. The second-neighbor shell consists of 12 Zn atoms: six at 3.196 Å, and six at 3.172 Å.

The details of the computational method are described in our previous papers,[33–35] and here we only mention some aspects specific for the present calculations. The calculations presented in this work were performed using the spin-polarized fully relativistic linear-muffin-tin-orbital (SPR LMTO) method[36,37] for the experimentally observed lattice constants $a = 9.588$ Å and $c = 5.16$ Å for wurtzite-type ZnO.[38] The crystal structure was optimized using the Vienna *ab initio* simulation package (VASP).[39–41] For LMTO and KKR calculations we used the Perdew-Wang[42] parameterization of the exchange-correlation potential. Brillouin zone (BZ) integrations were performed using the improved tetrahedron method[43] and charge self-consistentcy was obtained on a grid of 95 **k** points in the irreducible part of the BZ of the (Zn,V)O. To improve the potential we included additional interstitial spheres. The basis consisted of V and Zn s, p, and d; O s and p LMTOs.

X-ray absorption and dichroism spectra were calculated taking into account the exchange splitting of core levels. The finite lifetime of a core hole was accounted for by folding the spectra with a Lorentzian. The widths of the V L_2 and L_3 core level spectra, $\Gamma_{L_2} = 0.78$ eV and $\Gamma_{L_3} = 0.28$ eV, were taken from Ref. 44. The finite instrumental resolution of the spectrometer was accounted for by a Gaussian of width 0.6 eV.

The crystal structure obtained with the VASP code served as input in the calculations of exchange parameters using the magnetic force theorem as it is formulated within the KKR Green's function method.[45]

Since the local density approximation fails to describe correctly the strongly localized d state in ZnO we applied to these states the self-interaction correction (SIC) method as it is implemented in the multiple scattering theory.[46] This leads to a shift of the Zn d states downward in energy and makes the band gap larger (2.42 eV within the SIC vs 0.8 eV within the LDA in pure ZnO wurtzite).[47] The same effect can be achieved using a large U within the LDA + U method or treating the Zn d states as core states. In our LMTO calculations we tried both approaches and did not find any significant difference in the XAS and XMCD spectra. The V d states were treated within the LDA since they are located close to the Fermi level. In the vicinity of the Fermi level, the conventional local density approximation usually describes adequately occupied electronic states.[48] Nevertheless, in our simulations of XAS and XMCD spectra, we tried various U values within the LDA + U approach for the description of the V d states and found agreement between the theoretical and experimental results worse than within the LDA method.

III. RESULTS AND DISCUSSION

A. Simulations of XAS and XMCD spectra

The x-ray absorption and x-ray magnetic circular dichroism of the dilute magnetic semiconductor (Zn,V)O at the V $L_{2,3}$ edges have been investigated by Ishida *et al.* (Ref. 13). They found that ∼90% of the V ions were presumably strongly antiferromagnetically coupled, and the ferromagnetic component was below the detection limit of XMCD.

Since the real structure and chemical composition of $(Zn_{1-x}V_x)O$ was not known, we performed numerous calculations fitting XAS and XMCD spectra to the experimental results. The fitting parameters were positions of V atoms, Zn excess atoms, various oxygen vacancies, and the magnetic order of V atoms. The best fit is shown in Fig. 2, which presents the calculated XAS as well as XMCD spectra of the $(Zn_{1-x}V_x)O$ DMS (for $x = 0.1111$) at the V $L_{2,3}$ edges compared with the experimental data.[13] In this model, V atoms substitute cations and are antiferromagnetically ordered. Thereby, they are positioned at the largest possible V_1-V_2 distance of 5.53 Å (see Fig. 1). A relevant XMCD signal occurs only in the presence of an oxygen vacancy located in the first neighborhood shell of the second V_2 atom along the z direction (see Fig. 1). Adding Zn excess atoms also improves the agreement between the theory and the experiment.

The x-ray absorption spectrum at the V L_3 edge is rather complicated and consists of two major peaks c and d at 515.6 eV and 517 eV, respectively, with two additional low-energy shoulders a and b at 513.8 eV and 514.6 eV

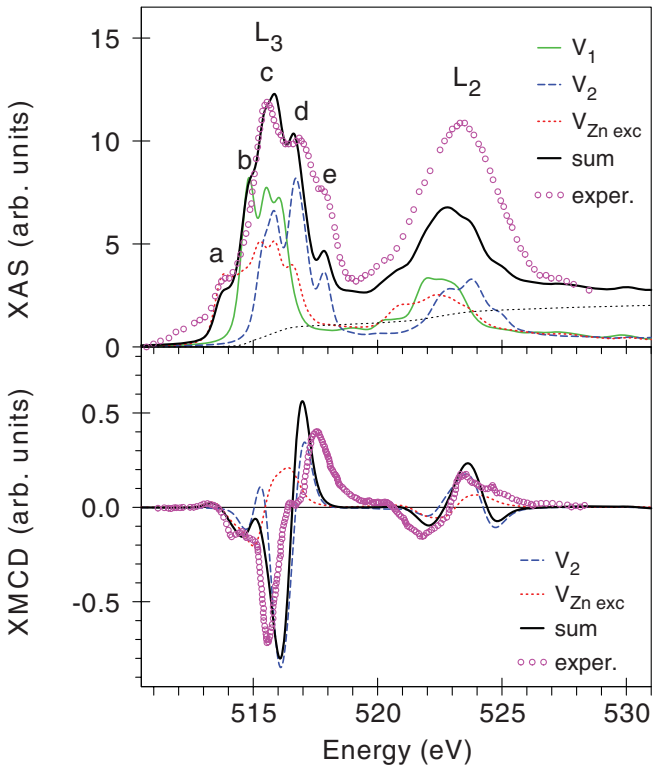

FIG. 2. (Color online) Top panel: theoretically calculated (thick full black line) and experimentally measured[13] (circles) x-ray absorption spectra of $(Zn_{1-x}V_x)O$ at the V $L_{2,3}$ edges. Full green line presents the x-ray absorption spectrum without any additional defects. Dashed blue and dotted red lines present the XA spectra with the oxygen vacancy (the contribution of the V_2 sublattice as in Fig. 1) and Zn excess atom, respectively. Bottom panel: theoretically calculated (thick full black line) and experimentally measured[13] (circles) XMCD spectra at the V $L_{2,3}$ edges. Dashed blue and dotted red lines present the XMCD spectra with the oxygen vacancy and Zn excess atom, respectively.

and a high-energy shoulder at 518 eV. As can be seen from the top panel of Fig. 2 the calculations for the ideal crystal structure with two substituted AFM-ordered V_1 atoms (full green curve) provide the x-ray absorption intensity only at peak *c* and shoulder *b*. The full explanation of the spectra is only possible by taking crystal imperfections into account.

We investigate the influence of two types of crystal defects on the XAS and XMCD spectra, namely, oxygen deficiency and Zn excess. We create an oxygen vacancy in the first neighborhood of the second V_2 atom along the *z* direction (see Fig. 1). The oxygen vacancy strongly affects the shape of the XAS spectra. As can be seen from Fig. 2 (top panel) the x-ray absorption from the V_2 atoms with the oxygen vacancy (blue dashed line) contributes to the major peak *c* and significantly determines the intensity of the peak *d* and the high-energy shoulder *e*. To investigate the Zn excess on the XMCD spectra we placed an extra Zn atom into the tetrahedral interstitial position 2.1916 Å apart from the V_2 site. The x-ray absorption from the $V_{\mathrm{Zn\,exc}}$ atoms with the Zn excess atom (red dotted line) contributes to the major peaks *c* and *d* as well as to both the low-energy shoulders *a* and *b*. Therefore, our simulation including oxygen deficiency and Zn excess reproduces the shape of the V L_3 x-ray absorption spectrum quite well (see thick black curve in top panel of Fig. 2). The lattice relaxation was found to be very important in the presence of the oxygen vacancy as well as the Zn excess. As discussed below, atomic relaxations around the vacancies cause a shift of the V_2 atom and three Zn atoms toward the vacant position. This shift affects hybridization between O $2p$ and V d states moving the states closer to the Fermi level.

Despite of the good agreement in the spectral shape and peak locations of the L_3 XAS, the theory fails to reproduce the experimentally observed L_3/L_2 XA ratio. It is well known, however, that the L_2 and L_3 absorption channels in early $3d$ transition metals with nearly empty d bands are strongly coupled through the photoelectron-core-hole Coulomb and exchange interactions.[49–52] This leads to a branching ratio close to 1:1, far from the statistical ratio 2:1, which is obtained in single-particle theory, unless the spin-orbit interaction in the final $3d$ band is considered. From our band structure calculations we obtained the L_3/L_2 branching ratio equal to 1.85 which is far from the experimentally observed value. This problem can be accounted for through many-electron calculations and we address it for future investigations.

The XMCD spectrum at the V L_3 edge is also rather complicated and consists of a small positive peak at 513.8 eV, a negative fine structure at 514.6 eV, a negative major peak at 515.6 eV, and a positive major peak at 517.7 eV with a shoulder at 516.4 eV. The V L_2 XMCD spectrum consists of two major fine structures, a negative peak at 521.8 eV, and a positive one at 523.3 eV. The theory is not able to reproduce the shape and relative intensity of the V $L_{2,3}$ XMCD spectra for the ferromagnetically ordered V atoms, with one and two V substitutions per unit cell. The theory strongly overestimates (from one to two orders of magnitude) the dichroism signal and produces a nonadequate shape of the spectra. On the other hand, the theory produces an almost vanishing XMCD signal for the AFM ordering of vanadium substitutional V ions for the ideal crystal structure without any kind of defects due to cancellation of the XMCD spectra with opposite spin directions.

We should mention that any shift from the antiferro- to the ferrimagnetic ordering will increase the intensity of the final XMCD spectra due to the reduction of the compensation of the XMCD spectra from V ions with opposite spin directions. Such a shift may be caused by an applied external magnetic field or different kinds of defects and imperfections in the lattice. The experimental measurements were performed in an external magnetic field of 7 T.[13] We have performed the calculations with an external magnetic field applied along the *z* direction and, indeed, obtained the spectra increase but only by approximately 10% to 20%. We found that only the defects cause a significant difference. As can be seen from the lower panel of Fig. 2 the theoretically calculated XMCD spectra with an oxygen vacancy (blue dashed line) resemble the experimental spectra quite well. An additional consideration of the Zn excess atoms (red dotted curve) leads to further improvement between theory and experiment.

One should mention that we obtain better agreement between the theory and the experiment in the x-ray absorption rather than in the XMCD spectra. The energy split between the two major peaks of the V L_3 XMCD spectrum was found to be smaller than the experimentally measured one. The reproduction of the shape of the V $L_{2,3}$ XMCD spectra is a quite difficult task because the rather weak final XMCD signal is derived from two large signals occurring from the V atoms with opposite spin directions. In this case, we have to take into account different crystal defects in a particular sample with quite precise relative concentration. However, the type and concentration of possible defects in the sample is not always well known. On the other hand, the extreme sensitivity of the XMCD signal may be considered as a useful tool to reveal the details of the composition, by modeling numerically different types of defects and comparing the theoretically calculated XMCD spectra with the experimentally measured ones. One way to improve the quality of theoretical simulations for such materials is the use of the coherent potential approximation,[53,54] and, in particular, the nonlocal coherent potential approximation,[55] which enables an efficient treatment of disorder including short-range effects.

B. Electronic structure of $(Zn_{1-x}V_x)O$

For a better understanding of electronic and magnetic properties the electronic structure of $(Zn_{1-x}V_x)O$ was studied in three different configurations: (i) the ideal wurtzite structure with ferromagnetically ordered V, and the model, elucidated from the XAS and XMCD experiments, with antiferromagnetically ordered V in presence of an oxygen vacancy in (ii) ideal and (iii) relaxed geometries.

Figure 3 presents total and partial density of states for a 36-atom ZnO wurtzite unit cell containing one V substitution ($x = 0.06$) in the local spin-density approximation (LSDA) [model (i)]. The O s states are located mostly between -21.0 and -19.7 eV below the Fermi level and the p states of the O are found between -9.6 eV and -3.0 eV. The spin splitting of the O p states is quite small. Zn d states occupy the energy interval between -9.6 and -3.0 eV and hybridize strongly with the O p states.

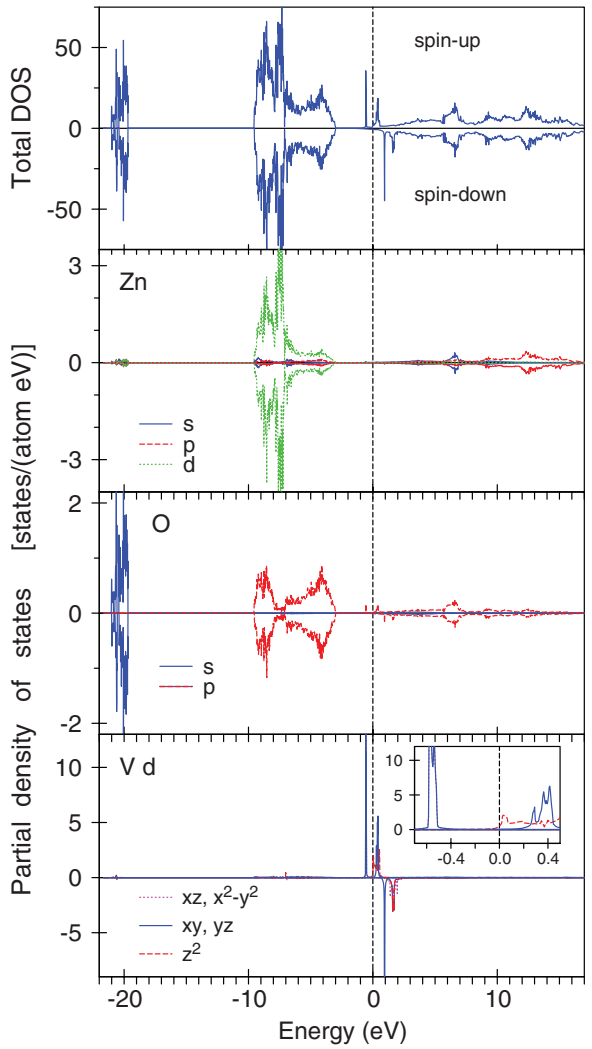

FIG. 3. (Color online) The LSDA total [in states/(cell eV)] and partial [in states/(atom eV)] densities of states, calculated by the LMTO method, for the O, Zn, and substituted V ions in $(Zn_{1-x}V_x)O$ [$x = 0.06$, model (i); see text for details]. The insert is a blowup of the V d PDOS close to the Fermi energy. The Fermi energy is at zero.

The crystal field at the V site (C_{3v} point symmetry) causes the splitting of V d orbitals into a singlet a_1 ($d_{3z^2-r^2}$) and two doublets e (d_{yz} and d_{zx}) and e_1 (d_{xy} and $d_{x^2-y^2}$). The majority-spin V $d_{3z^2-r^2}$ structure is found in close vicinity to the Fermi energy between -0.2 and 0.7 eV (see the insert in the bottom panel of Fig. 3). Very strong and narrow peaks of the majority-spin V bonding d_{xy} and d_{yz} states are located between -0.4 and -0.8 eV below the Fermi energy. The corresponding antibonding states are at 0.2 to 0.6 eV. Narrow peaks of the d_{xy}, and d_{yz} symmetry occur in the minority-spin channel at around 1 eV above the Fermi level. The energy interval of 1.4 to 2.2 eV above the Fermi level is occupied by the d_{zx}, $d_{x^2-y^2}$, and $d_{3z^2-r^2}$ states with minority spin.

The magnetic moment in the (Zn,V)O unit cell is 2.088 μ_B. Our band structure calculations yield the spin magnetic moment of 1.920 μ_B for the V atoms in $(Zn_{1-x}V_x)O$ ($x = 0.06$). The induced spin magnetic moments at the O first neighbor sites are of 0.004 μ_B and -0.003 μ_B for longer and shorter distant O atoms, respectively. Twelve Zn ions in the second neighbor shell couple ferromagnetically to the substituted V ion with spin magnetic moments of 0.034 μ_B to 0.068 μ_B. The orbital moments at the Zn and O sites are small with the largest one at the O first neighbor sites (0.001 μ_B). The orbital magnetic moment at the V site is -0.082 μ_B and is antiparallel to the spin moment.

We also investigated the electronic and magnetic structures of the $(Zn_{1-x}V_x)O$ DMSs with two of the Zn ions replaced by V. The supercell calculations were performed for the compositions $x = 0.1111$ (2/18), $x = 0.0625$ (2/32), and $x = 0.0555$ (2/36). We found that vanadium atoms substituted at different Zn sites show very little selectivity of site occupancy. Besides, different geometries with ferromagnetic and antiferromagnetic configurations are found to be energetically nearly degenerate; the difference in the total energies between ferromagnetic and antiferromagnetic solutions was found to be less than 3 meV per formula units. Still in most cases the ferromagnetic solution is lower in total energy in comparison with the antiferromagnetic solution. Similar results were reported earlier by Wang *et al.* (Ref. 20). However, for the fully relaxed lattice we found that the AFM ordering has lower total energy in comparison with the FM one.

Figure 4 presents vanadium d and oxygen p partial densities of states for the $(Zn_{1-x}V_x)O$ wurtzite unit cell containing two V substituted atoms ($x = 0.1111$) ordered antiferromagnetically plus oxygen vacancy near the V_2 atom (see Fig. 1), in close vicinity to the Fermi level. The oxygen vacancy has four nearest-neighbor atoms: three Zn atoms at the distance of 1.9496 Å and one V atom at 1.9505 Å. The vacancy does not affect the energy distribution of the partial DOS much without taking the lattice relaxation into account [model (ii); full blue lines in Fig. 4]. However, it strongly affects the shape and energy position of the partial DOS for the relaxed lattice [model (iii); dashed red curves], placing V_2 d states right to the Fermi level and V_1 d states in its close vicinity. The lattice relaxation causes the shift of the V_2 atom and three Zn atoms toward the vacant site by 0.14 Å and 0.26 Å, respectively.

C. Exchange interactions in $(Zn_{1-x}V_x)O$

To describe the magnetic properties of $(Zn_{1-x}V_x)O$ we calculated exchange interactions between magnetic moments using the magnetic force theorem as it is implemented within the multiple scattering theory:[45]

$$J_{ij} = \frac{1}{4\pi}\int^{\varepsilon_F} d\varepsilon\, \mathrm{Im}\,\mathrm{Tr}_L[\Delta_i(\varepsilon)G^{ij}_{\uparrow}(\varepsilon)\Delta_j(\varepsilon)G^{ji}_{\downarrow}(\varepsilon)]. \quad (1)$$

Here, Tr_L denotes the trace over the angular momentum, $G^{ij}_{\sigma}(\varepsilon)$ is the backscattering operator of a spin σ between sites i and j, and $\Delta_i(\varepsilon) = t^i_{\uparrow}(\varepsilon) - t^i_{\downarrow}(\varepsilon)$ is defined via the single scattering path operators t^i_{σ} and closely related to the exchange splitting corresponding to the magnetic atom i. Exchange parameters calculated for a certain reference state provide usually a reliable hint about the ground-state magnetic structure. Our tests yielded very similar results for J_{ij} in both ferromagnetic and antiferromagnetic reference states. However, the exchange parameters, presented in this study, were calculated in that

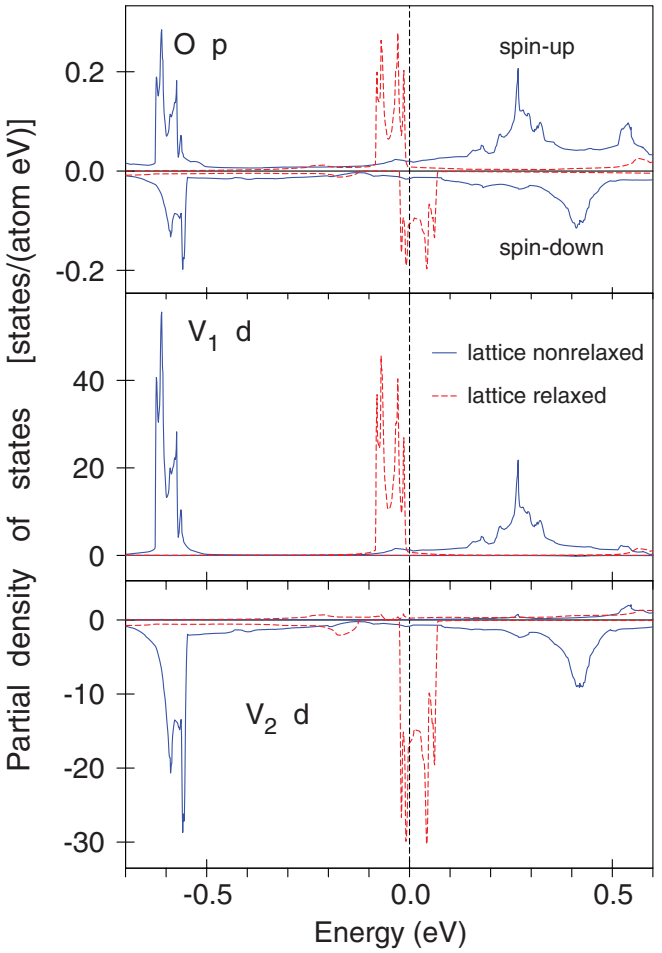

FIG. 4. (Color online) The LSDA d-partial [in states/(atom eV)] densities of states, calculated by the LMTO method, for the substituted V_1 and V_2 ions in $(Zn_{1-x}V_x)O$ middle and lower panels, respectively (see the explanation in the text). Upper panel presents O p partial density of states. Full blue and dashed red lines show the results for nonrelaxed [model (ii)] and relaxed [model (iii)] lattices. The Fermi energy is at zero.

reference state, which was found to have the lowest total energy.

The exchange parameters J_{ij} defined by Eq. (1) can be used to estimate the characteristic temperature of magnetic ordering in $(Zn_{1-x}V_x)O$ within the effective Heisenberg Hamiltonian

$$H = -\sum_{i,j} J_{ij}\mathbf{e}_i \cdot \mathbf{e}_j \,, \tag{2}$$

using a random-phase approximation for the magnon Green's function.[56] Here, $\mathbf{e}_i$ is a unit vector parallel to the magnetic moment at site i.

The structural model, elucidated from our XAS and XMCD simulations, was utilized for calculations of the corresponding electronic structure and exchange parameters using the KKR Green's function method in the multiple scattering representation.[35] The schematic representation of the exchange interaction between the magnetic moments of the nearest neighbors is shown in Fig. 5.

The strongest magnetic interactions were found between V atoms only if there is either an oxygen atom or an oxygen

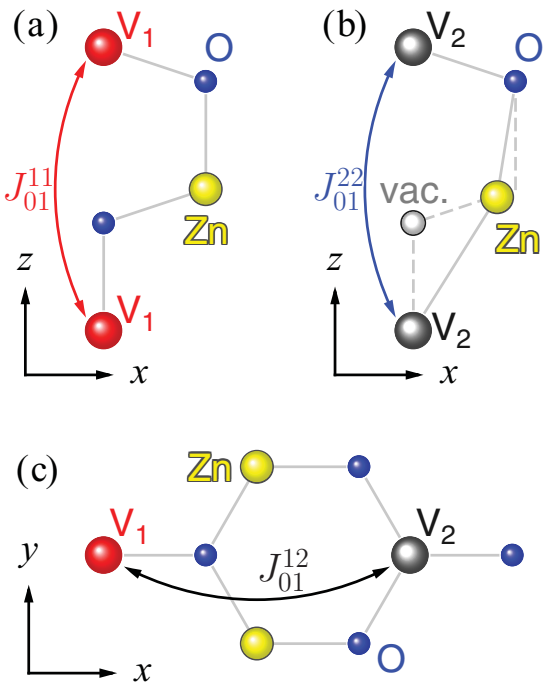

FIG. 5. (Color online) Schematic representation of magnetic interactions between V atoms in $(Zn_{1-x}V_x)O$. (a) Two V atoms substituting Zn positions with an oxygen in between. (b) Two V atoms within an oxygen vacancy in between. (c) V_1-V_2 pair (see the text for explanation). The dashed line in (b) shows ideal wurtzite structure.

vacancy in between [see Figs. 1, 5(a) and 5(b), respectively). Thereby, one can distinguish two different vanadium atoms: V_1 far from and V_2 close to an oxygen vacancy. The exchange interaction between V_1 and V_2 atoms is very small since the atoms are separated by 5.53 Å and there is no connecting atom in between [see Figs. 1 and 5(c)]. The exchange interaction in V_1-V_1 is mediated mainly by the oxygen between the vanadium atoms and is positive leading to a ferromagnetic order in this pair [see J_{01}^{11} at zero relaxation in Fig. 6(b)]. This changes by replacing the oxygen by a vacancy (V_2-V_2 pair) in accordance to our structural model. Removing the oxygen atom kills the exchange interaction between the neighboring vanadium moments [see J_{01}^{22} at zero relaxation in Fig. 6(b)]. However, the atoms around the vacancy experience strong relaxations and this promotes an antiferromagnetic order in this pair. Our simulations show that the exchange interaction is very sensitive to these atomic movements. We found that most substantial changes of J_{ij} occur when the neighboring Zn atoms move toward the vacancy (see inset in Fig. 6), while relaxations of V and O atoms are insignificant for the magnetic interaction. According to our structural optimizations the shift of the Zn atoms is about 0.26 Å. Due to these relaxations, the exchange parameters between the first neighbors J_{01}^{22} were changed from $\approx$0 meV in the nonrelaxed geometry to -16 meV. The interaction between the second neighbors experiences as well significant changes and is positive at the relaxed geometry. This suggests that the V_2-V_2 pair with an oxygen vacancy is antiferromagnetic. The vanadium pairs V_1-V_1 without oxygen vacancies remain

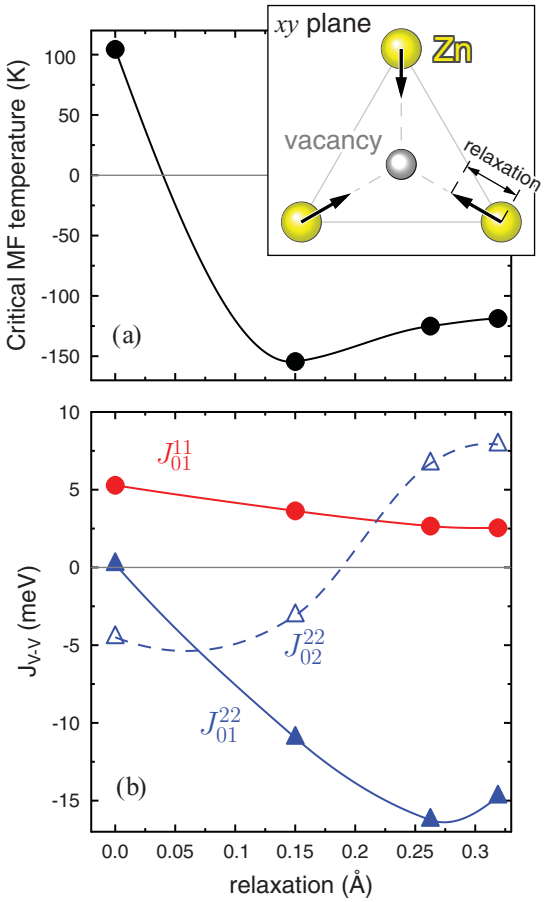

FIG. 6. (Color online) Critical temperatures (a) and exchange parameters (b) for $(Zn_{1-x}V_x)O$ calculated for various positions of atoms around an oxygen vacancy. Inset shows scheme of movements of Zn atoms toward to the vacancy.

ferromagnetic, although the value of the exchange parameters J_{01}^{11} reduces from 5.8 meV in the nonrelaxed case to 2.6 meV after relaxation. The critical temperature, estimated within the random-phase approximation, is about 120 K in the relaxed geometry.

The most important question is why the relaxations of Zn atoms around the vacancy lead to such substantial changes of magnetic interactions. The Zn states are deep in the valence bands and do not hybridize with the V states which are located close to the Fermi level (see Fig. 3). Relaxations of oxygen atoms were found to be very small and do not change magnetic properties of $(Zn_{1-x}V_x)O$. However, the hybridization between V $3d$ and oxygen $2p$ states is strongly affected by the relaxations of the Zn atoms (see the partial DOS in Fig. 4), which is evidently crucial for the magnetic interactions in this system. Our analysis of the DOS and occupation numbers yields a significant increase of the hybridization between V $3d$ and O $2p$ states. This is governed by stronger d-d hybridization between Zn atoms moved toward the vacancy and, at the same time, due to decreasing the hybridization between these Zn $3d$ and O $2p$ states.

IV. SUMMARY

We have studied the electronic structure and x-ray magnetic circular dichroism of the (Zn,V)O dilute magnetic semiconductors, by means of the *ab initio* fully relativistic spin-polarized Dirac linear muffin-tin orbital method in the framework of the LSDA approximation. The x-ray absorption and dichroism spectra at the V $L_{2,3}$ edges were investigated.

The shape of the V $L_{2,3}$ XMCD spectra might be explained only by suggesting the AFM ordering between the V ions situated at the largest possible $V^{\uparrow}$-$V^{\downarrow}$ distance from each other for the concentration $x = 0.1111$. The XMCD signal appears as superposition of very intensive dichroic signals from V ions with opposite spin directions. The relevant XMCD signal is obtained only in the presence of an oxygen vacancy located in the first neighborhood of the second V atom. Adding extra Zn atoms improves the agreement between the theory and the experiment as well. The lattice relaxation was found to be very important in the presence of the oxygen vacancy as well as Zn excess.

The structure obtained from the comparison of the XMCD spectra and theoretical simulations was used to study magnetic properties of (Zn,V)O DMSs. Using the magnetic force theorem as it is implemented within the multiple scattering theory, we have calculated the exchange parameters of the magnetic interaction between the V atoms. We have found that magnetic V ions form two magnetic pairs, one ferromagnetic and another antiferromagnetic, which interact weakly with each other. The antiferromagnetic order in one of the pairs is due to the presence of an oxygen vacancy and strongly relaxed positions of neighboring Zn atoms.

ACKNOWLEDGMENTS

L.V.B. gratefully acknowledges the hospitality at Max-Planck-Institut für Mikrostrukturphysik in Halle during his stay there. V. N. A. gratefully acknowledges the hospitality at Max-Planck-Institut für Festkörperforschung in Stuttgart during his stay there. This work was supported by the Science and Technology Center of Ukraine (STCU), Project No. 4930, and by the *Sonderforschungsbereich* SFB 762, "Functionality of Oxide Interfaces." Some of the calculations were performed at the Rechenzentrum Garching of the Max Planck Society (Germany).

*v.antonov@fkf.mpg.de
†aernst@mpi-halle.de

[1]H. Cao, Z. Pei, J. Gong, C. Sun, R. Huang, and L. Wen, J. Solid State Chem. **177**, 1480 (2004).
[2]T. Dietl, H. Ohno, F. Matsukura, J. Cibert, and D. Ferrand, Science **287**, 1019 (2000).
[3]K. Ueda, H. Tabata, and T. Kawai, Appl. Phys. Lett. **79**, 988 (2001).

[4]C. Liu, F. Yun, and H. Morko, J. Mater. Sci.: Mater. Electron. **16**, 555 (2005).
[5]H. Saeki, H. Tabata, and T. Kawai, Solid State Commun. **120**, 439 (2001).
[6]Y. Ishida, J. Hwang, M. Kobayashi, A. Fujimori, H. Saeki, H. Tabata, and T. Kawai, Physica B: Condensed Matter **351**, 304 (2004).
[7]N. H. Hong, J. Sakai, and A. Hassini, J. Appl. Phys. **97**, 10D312 (2005).
[8]N. H. Hong, J. Sakai, and A. Hassini, J. Phys. Condens. Matter **17**, 199 (2005).
[9]M. Venkatesan, C. B. Fitzgerald, J. G. Lunney, and J. M. D. Coey, Phys. Rev. Lett. **93**, 177206 (2004).
[10]J. R. Neal, A. J. Behan, R. M. Ibrahim, H. J. Blythe, M. Ziese, A. M. Fox, and G. A. Gehring, Phys. Rev. Lett. **96**, 197208 (2006).
[11]H. Saeki, H. Matsui, T. Kawai, and H. Tabata, J. Phys. Condens. Matter **16**, S5533 (2004).
[12]S. Ramachandran, A. Tiwari, J. Narayan, and J. T. Prater, Appl. Phys. Lett. **87**, 172502 (2005).
[13]Y. Ishida *et al*., Appl. Phys. Lett. **90**, 022510 (2007).
[14]S. Zhou, K. Potzger, H. Reuther, K. Kuepper, W. Skorupa, M. Helm, and J. Fassbender, J. Appl. Phys. **101**, 09H109 (2007).
[15]S. Yuming, X. Pengshou, S. Chaoshu, X. Faqiang, P. Haibin, and L. Erdong, J. Electron Spectrosc. Relat. Phenom. **114–116**, 1123 (2001).
[16]K. Sato and H. Katayama-Yoshida, Phys. Status Solidi B **229**, 673 (2002).
[17]K. Sato and H. Katayama-Yoshida, Semicond. Sci. Technol. **17**, 367 (2002).
[18]Y. Uspenskii, E. Kulatov, H. Mariette, H. Nakayama, and H. Ohta, J. Magn. Magn. Mater. **258-259**, 248 (2003).
[19]B. Kang, W. Kim, Y. Shong, and H. Kang, J. Cryst. Growth **287**, 74 (2006).
[20]Q. Wang, Q. Sun, P. Jena, Z. Hu, R. Note, and Y. Kawazoe, Appl. Phys. Lett. **91**, 063116 (2007).
[21]M. H. Sukkar and H. L. Tuller, in *Advances in Ceramics*, edited by M. F. Yan and A. H. Heuer, Vol. 7 (American Ceramics Society, Columbus, OH, 1983), pp. 71–90.
[22]G. D. Mahan, J. Appl. Phys. **54**, 3825 (1983).
[23]K. I. Hagemark, J. Solid State Chem. **16**, 293 (1976).
[24]J. S. Choi and C. H. Yo, J. Phys. Chem. Solids **37**, 1149 (1976).
[25]A. W. Sleight and R. Wang, in *Solid-State Chemistry of Inorganic Materials*, edited by P. K. Davies, A. J. Jacobson, C. C. Torardi, and T. A. Vanderah (Materials Research Society, Pittsburgh, 1996), Vol. 453 of MRS Symposia Proceedings, pp. 323–330.
[26]J. W. Hoffman and I. Lauder, Trans. Faraday Soc. **66**, 2346 (1970).
[27]E. Ziegler, A. Heinrich, H. Oppermann, and G. Stöver, Phys. Status Solidi A **66**, 635 (1981).
[28]A. Janotti and C. G. Van de Walle, Rep. Prog. Phys. **72**, 126501 (2009).
[29]R. Vidya, P. Ravindran, H. Fjellvag, B. Svensson, E. Monakhov, M. Ganchenkova, and R. Nieminen, Phys. Rev. B **83**, 045206 (2011).
[30]A. F. Kohan, G. Ceder, D. Morgan, and C. G. Van de Walle, Phys. Rev. B **61**, 15019 (2000).
[31]Y.-S. Kim and C. Park, Phys. Rev. Lett. **102**, 086403 (2009).
[32]S. H. Liu, H. S. Hsu, C. R. Lin, C. S. Lue, and J. C. A. Huang, Appl. Phys. Lett. **90**, 222505 (2007).
[33]V. N. Antonov, H. A. Dürr, Y. Kucherenko, L. V. Bekenov, and A. N. Yaresko, Phys. Rev. B **72**, 054441 (2005).
[34]V. N. Antonov, A. N. Yaresko, and O. Jepsen, Phys. Rev. B **81**, 075209 (2010).
[35]M. Luders, A. Ernst, W. M. Temmerman, Z. Szotek, and P. J. Durham, J. Phys. Condens. Matter **13**, 8587 (2001).
[36]O. K. Andersen, Phys. Rev. B **12**, 3060 (1975).
[37]V. V. Nemoshkalenko, A. E. Krasovskii, V. N. Antonov, V. N. Antonov, U. Fleck, H. Wonn, and P. Ziesche, Phys. Status Solidi B **120**, 283 (1983).
[38]S. Saib and N. Bouarissa, Physica B **387**, 377 (2007).
[39]P. E. Blöchl, Phys. Rev. B **50**, 17953 (1994).
[40]J. P. Perdew, K. Burke, and M. Ernzerhof, Phys. Rev. Lett. **78**, 1396 (1997).
[41]G. Kresse and D. Joubert, Phys. Rev. B **59**, 1758 (1999).
[42]J. Perdew and Y. Wang, Phys. Rev. B **45**, 13244 (1992).
[43]P. E. Blöchl, O. Jepsen, and O. K. Andersen, Phys. Rev. B **49**, 16223 (1994).
[44]J. L. Campbell and T. Parr, At. Data Nucl. Data Tables **77**, 1 (2001).
[45]A. I. Liechtenstein, M. I. Katsnelson, V. P. Antropov, and V. A. Gubanov, J. Magn. Magn. Mater. **67**, 65 (1987).
[46]M. Lüders, A. Ernst, M. Däne, Z. Szotek, A. Svane, D. Ködderitzsch, W. Hergert, B. L. Györffy, and W. M. Temmerman, Phys. Rev. B **71**, 205109 (2005).
[47]I. V. Maznichenko *et al*., Phys. Rev. B **80**, 144101 (2009).
[48]L. J. Sham and W. Kohn, Phys. Rev. **145**, 561 (1966).
[49]J. Zaanen, G. A. Sawatzky, J. Fink, W. Speier, and J. C. Fuggle, Phys. Rev. B **32**, 4905 (1985).
[50]J. Schwitalla and H. Ebert, Phys. Rev. Lett. **80**, 4586 (1998).
[51]P. Krüger and C. R. Natoli, Phys. Rev. B **70**, 245120 (2004).
[52]A. L. Ankudinov, A. I. Nesvizhskii, and J. J. Rehr, Phys. Rev. B **67**, 115120 (2003).
[53]P. Soven, Phys. Rev. **156**, 809 (1967).
[54]B. L. Gyorffy, Phys. Rev. B **5**, 2382 (1972).
[55]D. A. Rowlands, A. Ernst, B. L. Györffy, and J. B. Staunton, Phys. Rev. B **73**, 165122 (2006).
[56]S. V. Tyablikov, *Methods of Quantum Theory of Magnetism* (Plenum Press, New York, 1967).